A multidisciplinary approach in sinkhole analysis: The Quinis village case study (NE-Italy)

Luca Zini, Chiara Calligaris *, Emanuele Forte, Lorenzo Petronio, Enrico Zavagno, Chiara Boccali, Franco Cucchi

Department of Mathematics and Geosciences, University of Trieste - Itlay Lorenzo Petronio, OGS - National Institute of Oceanography and Experimental Geophysics, Italy

ARTICLE INFO

Accepted 3 July 2015

Keywords:
Sinkholes
Gypsum
Karst
Hydrogeology
Geophysical investigations

ABSTRACT

During the last recent years, in Quinis, a small village sited in the Alta Val Tagliamento valley (Friuli Venezia Giulia Region, NE Italy), the inhabitants faced with instability phenomena related to the presence of soluble rocks in the subsurface. The evaporite bedrock is mainly mantled, in fact, by high thickness deposit. This paper explains the methodological approach that we used to identify the instabilities in a very complex geo-structural environment where the urbanization limits the applicability of several investigation techniques. Different methods were used to define the bedrock morphology, to characterize the mantling deposits and to identify the processes behind. What emerged from the study is a mandatory multidisciplinary approach to characterize the subsoil, because each technique is not able individually to take to a unique result. The data collected allowed to draft a geo–hydrogeological conceptual model of the Quinis village.
The lessons learned, even if with some site-specific dependency, demonstrate the importance of broad-spectrum investigations, which are essential to understand the subsurface characteristics avoiding relevant socio-economic impact and supporting an adequate future territorial planning.

1. Introduction

Sinkholes are a common geological feature in soil-covered karst areas. The term has a genetic connotation (Waltham et al., 2005) indicating a depression where the ground and/or water sink. The different types of sinkholes are primarily described using the dominant processes behind their development and/or the material involved (Beck, 2004; Waltham et al., 2005; Gutiérrez et al., 2008, 2014). They may include sudden catastrophic collapses, which may be more frequent and rapid in evaporites than in carbonate rocks due to the former's higher solubility rate and lower mechanical strength (Cucchi and Forti, 1993; Cucchi et al., 1994; Klimchouk et al., 1996; Dreybrodt and Eisenlohr, 2000; Jeschke et al., 2001; Waltham et al., 2005; Ford and Williams, 2007; Furlani et al., 2009). At the human time scale, the high solubility of the evaporites favour the development of unstable voids that may be extremely problematic due to the severe damage they can cause on man-made structures (Klimchouk et al., 1996; Cooper and Calow, 1998; Cooper and Waltham, 1999; Benson and Kaufmann, 2001; Gutiérrez and Cooper, 2002; Guerrero et al., 2004; Waltham et al., 2005; Gutiérrez et al., 2008; Galve et al., 2009a; Iovine et al., 2010). Within this framework, the application of effective remedial measures is usually very difficult, especially when the voids, located at considerable depths, cause rapid subsidence (Gutiérrez et al., 2009, 2014). Land-use planning in sinkhole-prone areas needs to be preceded by detailed investigations focused on the identification of pre-existing sinkholes, subsurface dissolution and subsidence features (Soriano and Simon, 1995; Nisio et al., 2007; Galve et al., 2009b; Parise and Vennari, 2013). The avoidance of these areas is the safest and commonly most cost-effective sinkhole risk mitigation strategy (Gutiérrez et al., 2008), but frequently not the most popular. When sinkholes may adversely interact with the human environment, multidisciplinary approaches should be planned to i) locate the subsurface dissolution and subsidence features; ii) define precisely the limits of the sinkholes and the underlying subsidence structures; iii) understand the causes of the deformation; and iv) assess and predict the kinematics of the subsidence phenomena, in particular as regards potential episodes of catastrophic collapse. Field surveys, interpretation of remote-sensed imagery and spatial and temporal analyses are often useful to identify obliterated sinkholes causal factors (Forth et al., 1999; Kaufmann and Quinif, 2002; Brinkmann et al., 2007, 2008; Gutiérrez et al., 2008). Hydrogeological investigations are commonly a crucial aspect for understanding the genesis and evolution of sinkholes (Gutiérrez et al., 2008). The position of the groundwater table and its fluctuations through time and space (Lamont-Black et al., 2005), obtained primarily by using long-term piezometric data (Cooper and Calow, 1997; Wanfang, 1997), is essential to estimate the groundwater flow patterns and the development of the depression causes, which may play a fundamental role in the formation of sinkholes.

Geophysical methods also have been widely used for the study of sinkholes and the detection of the underground voids linked to their development (e.g., Van Schoor, 2002; Kaufmann et al., 2011) or to identify and outline, within larger areas, the zones most susceptible to sink

* Corresponding author.

(e.g., Krawczyk et al., 2011; Margiotta et al., 2012). To obtain subsurface information about the near-surface materials with non–invasive techniques, the highest resolution is achieved using Ground Penetrating Radar (GPR) techniques (Marcak et al., 2008; Gutiérrez et al., 2009; Pueyo-Anchuela et al., 2009; Gutiérrez et al., 2011; Ercoli et al., 2013). Electrical Resistivity Tomography (ERT) and other active or passive electrical methods, such as self-potential (SP) and electromagnetic (EM) surveys, are often used to investigate the subsurface at different depths that ordinarily do not exceed 100 m (e.g., Van Schoor, 2002; Jardani et al., 2007; Ezersky, 2008; Pepe et al., 2015).

Reflection and refraction seismic methods are widely applied to reach depths of several hundred meters or greater (Steeples et al., 1986; Grandjean and Leparoux, 2004; Krawczyk et al., 2011). Gravimetric surveys are also effective for locating subsurface voids (e.g., Butler, 1984; Dahm et al., 2010).

The effectiveness of each technique depends on its ability to reach the target depth with the appropriate resolution in different geological settings. Therefore, integrated geophysical approaches are often reported as well as the calibration/validation with information obtained directly from boreholes (Dobecki and Upchurch, 2006; Cardarelli et al., 2010; Delle Rose and Leucci, 2010; Kaufmann et al., 2011; Margiotta et al., 2012; Pepe et al., 2013; Cardarelli et al., 2014) or trenches (Gutiérrez et al., 2009).

In this paper the Authors analyse a small area located in the Quinis village (Friuli Venezia Giulia Region, NE Italy), applying and integrating multiple techniques to define the causes and dynamics of the evaporite dissolution-induced subsidence phenomena that cause damages to the existing infrastructures, and to better define the applicability of these techniques. In the north-eastern side of Italy, about 40.000 people, in more than 30 municipalities are living in situations similar to the Quinis

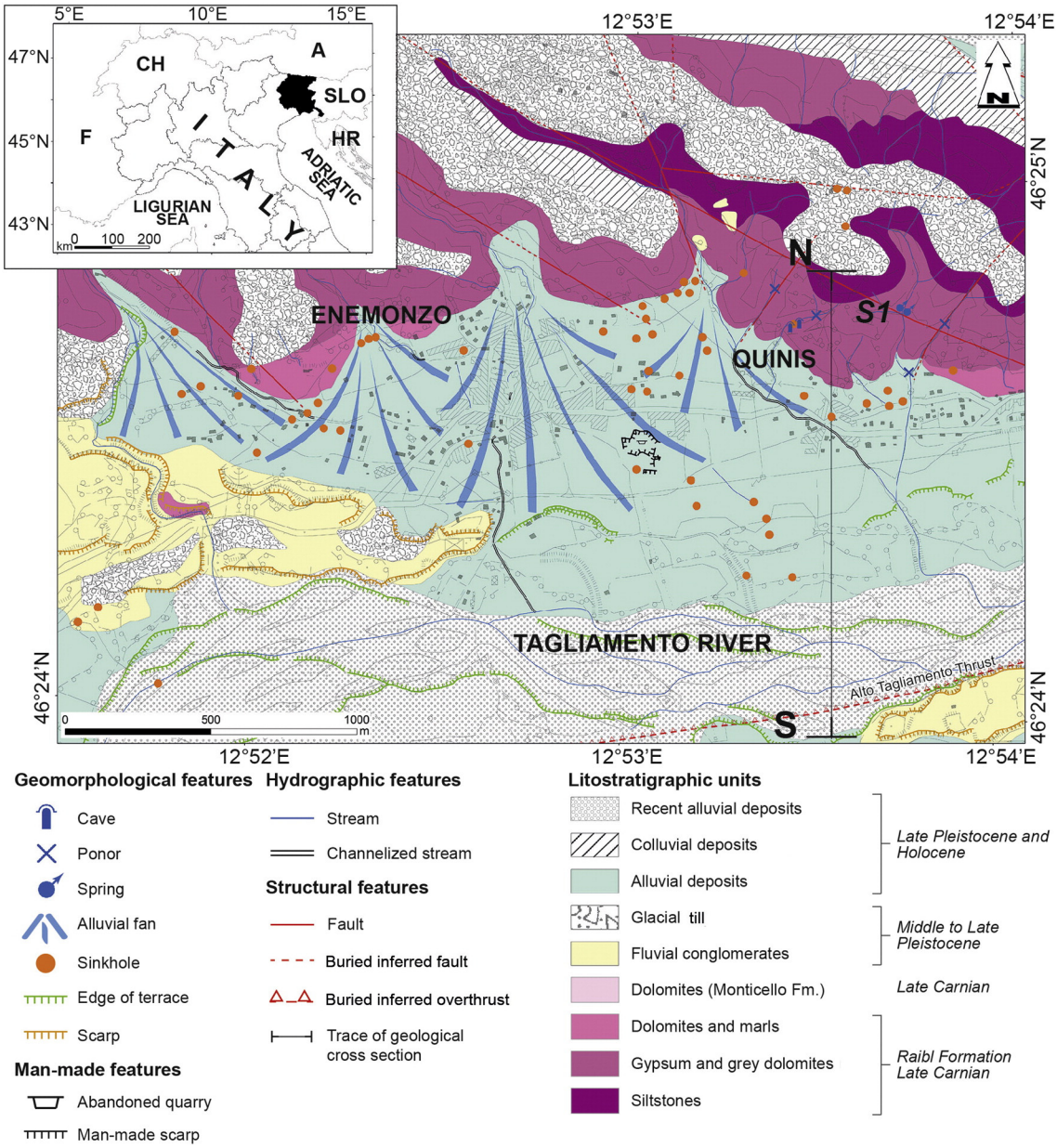

Fig. 1. Geological map of the study area.
(Modified after Venturini, 2009).

one. The experiences acquired and the outcomes obtained could be later used to better understand similar environments.

2. Study area

The study area is located in the mountain sector of Friuli Venezia Giulia Region, NE Italy, along the Tagliamento River valley. Here, dissolution and subsidence processes are related to the presence of evaporites (Fig. 1). The Enemonzo municipality, and especially the Quinis village, with their numerous sinkholes, are a representative example of the complex regional geological situation typical of the northeastern Italian valleys, which at present it is still not fully understood.

In the region there are two meaningful evaporitic units deposited one in the Permian and the other in the Triassic. The Late Permian Bellerophon Formation consists of dolostones, marls and evaporites (gypsum and anhydrite). Due to intense Alpine tectonic deformation and the presence of extensive cover deposits, it seldom crops out (Carulli, 2006; Venturini, 2009).

During the Triassic, the tectono-eustatic sea-level fluctuations controlled the cyclic deposition of the Raibl Formation (Late Carnian), comprising evaporitic intervals (Bechstadt and Schweizer, 1991) of saccharoid gypsum with abundant millimetric clay lenticular layers and metric to decimetric alternations of marly and vacuolar dolomites (Carulli, 2006). The evaporitic Raibl Formation is widespread in the region and especially in the study area, where it crops out north of Quinis village (Brusca et al., 1982; Burelli et al., 2004; Calligaris et al., 2009; Cucchi and Piano, 2002; Venturini, 2009). From base to top (Fig. 1), it consists in: a) red siltstones Member, primarily composed of shales and siltstones, 80–100 m thick; b) gypsum and grey dolomites Member, with an estimated thickness of 350 m; c) dolomites and marls Member, including dolomites, marly dolomites, marls and rare multicolour shales, around 180 m thick (Venturini, 2009).

The Quaternary deposits, Late Pleistocene–Holocene in age, mantling the 99% of the evaporites, consist of glacial till, alluvial and colluvial deposits. On the southern side of Enemonzo–Quinis, these deposits overlap the fluvial conglomerates of the Middle–Late Pleistocene. These materials are extremely heterogeneous due to a complex and articulated depositional patterns conditioned by several factors including the tectonical setting, the alternation of glacial and interglacial periods, the recent depositional events due to the Tagliamento River (recent alluvial deposits) and the overlapping alluvial fan present in the northern sector.

The highly permeable, polygenic gravels (recent alluvial deposits and alluvial deposits), include lenticular intercalations of less pervious clay and clayey-silt. Although the gravels are locally cemented primarily close to the Tagliamento riverbed, the geotechnical characteristics of the whole alluvial deposits are quite poor, with a high vertical and horizontal variability of the bearing capacity.

The most important tectonic feature in the area is the S-verging "Alto Tagliamento" overthrust, primarily E-W oriented, that separates the "Alpi Tolmezzine" (Northern sector) from the "Prealpi Carniche" (Southern sector), taking the Raibl Formation in the hanging-wall to overthrust the Monticello Formation. This structure, buried in the study area and recognisable only to the West, dips approximately 60° to the NW. Other smaller faults, with a quite penetrative NW–SE trend, are present in the area (Venturini, 2009).

LiDAR data with a spatial resolution of 1 m allowed the recognition of some sinkholes and, in the piedmont of the hills located north of Quinis village, highlighted the presence of a system of coalescing alluvial fans (Fig. 1). In the southern part of the area, the Tagliamento River with its E-W oriented course develops along one of the primary thrusts of the South Alpine domain (along the "Alto Tagliamento" overthrust). The valley floor consists of a wide braided channel flanked by terraces (Fig. 1). Quinis is located on deposits characteristics of alluvial fans that prograded over the fluvial terrace of the Tagliamento River.

3. Materials and methods

To obtain information on the distribution and frequency of the sinkhole phenomena, a detailed investigation was performed using as starting point the first cartographic inventory of sinkholes in the Quinis area (Fig. 2). Data obtained from oral witnesses, technical documents (Floreani and Jaiza, 1980), field surveys and LiDAR joined the Geodatabase. The sinkholes were classified following the scheme proposed by Gutiérrez et al. (2008, 2014), whereby sinkholes are described indicating the material affected by subsidence (cover, bedrock and caprock) and the subsidence mechanism (collapse, suffosion, sagging).

Regarding the events in the Enemonzo municipality and in the surroundings, the first reports on sinkholes date back to the end of the 19th century (Marinelli, 1898). At Quinis, a meaningful incident is related to the church and its bell tower. The church was built in the 17th century and restored several times due to instability problems until the 1970s when, before the earthquake cluster of 1976, with its two main events on May 6 and September 15 (moment magnitudes of 6.4 and 6.0, respectively) the church was demolished due to the collapse risk. The bell tower was built in 1903, but in 1920, the tilting led to a first restoration for safety reasons. At the present time, the structure is inclined, and its base has been reinforced to increase the stability.

In the 1960s, an increase in the frequency of sinkhole events was recorded just after the exploitation of the Tagliamento River for hydroelectric purposes (Gortani, 1965), with the occurrence of at least five large sinkholes up to 45 m across (Table 1). Gortani (1965) reported that these events occurred just after a groundwater level lowering of up to 4 m recorded by a piezometer located at Invillino, approximately 4 km SE of Enemonzo (Ufficio Idrografico del Magistrato delle acque, 1966).

During the sixties and seventies, several houses were demolished or restored due to severe damage caused by sinkholes. The largest earthquake of the last century that struck the region in 1976 aggravated the damage in human structures, but it seems that it did not trigger new sinkholes. In 1985, in Enemonzo, a new sinkhole caused the demolition of three houses (Table 1). Since 2000, a new phase of sinkholes formation has occurred in Quinis village. The present paper considers only the larger events that were clearly identified and examined in the field. Data on small sinkholes are less precise and many of these depressions are filled by the local people soon after they form.

3.1. Borehole data and geotechnical measurements

Between 2005 and 2013, a total of 25 boreholes were drilled in a selected sector of Quinis village (Fig. 3), twenty of which were drilled cores and five rotary drilled wells. These direct investigations provide information on the stratigraphic characteristics of both the soil-cover and the bedrock, as well as the presence of voids and low bearing capacity layers. Boreholes also allow calibrating and validating the geophysical investigations. Twelve boreholes reached the rockhead of the gypsum unit; the remaining thirteen boreholes penetrated well below the gypsum rockhead reaching a depth up to 81.1 m below ground level (PZ22). Twenty-two boreholes were equipped with piezometers. The thicknesses and position of the screens were defined on the basis of hydrogeological considerations (permeability): nine screens filtered the deposits or the weathered upper part of the gypsum unit, while the others were located within the gypsum bedrock. Two boreholes were equipped with a SISGEO (2005) magnet extensometer (A12 and A13) working using the British Building Research technique. PZ19 has been dedicated to geophysical investigations. Periodic extensometric acquisition started in May 2011. A12 extensometer is equipped with 29 spider magnets placed at 1 m of distance one from each other (from 1 m to 38.5 m depth) and A13 with 33 (from 1.5 m to 33.2 m depth). Each measuring survey consists in the acquisition of the depth of each single spider magnet with respect to a fixed reference point outside.

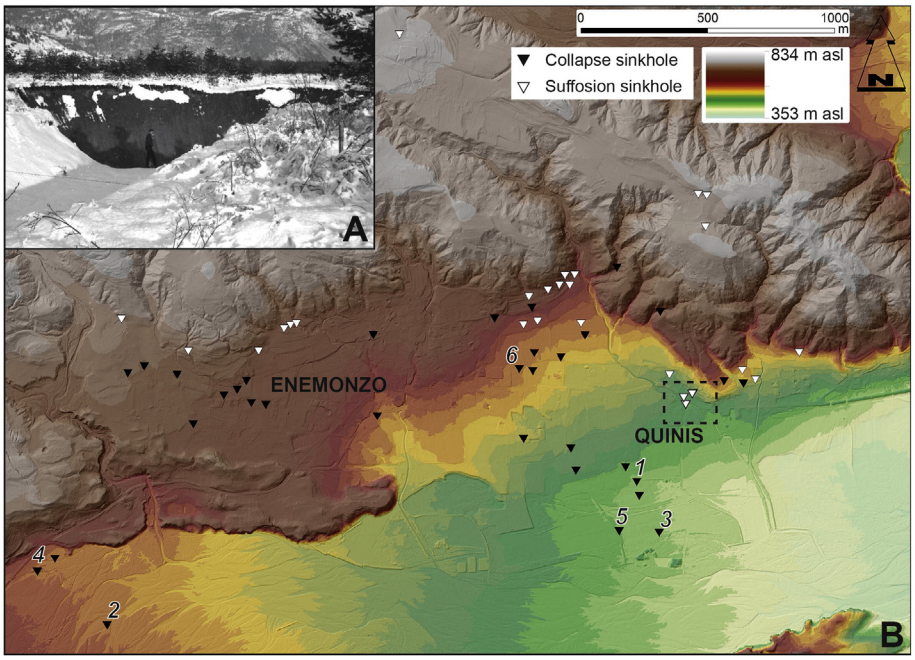

Fig. 2. A) Cover collapse sinkhole (5) occurred in 1963 and described by Gortani (1965). B) DEM of the area affected by sinkholes. Cover collapse sinkholes (white triangles) and cover suffosion sinkholes (black triangles). Numbered sinkholes are cited in Table 1.

From the geotechnical point of view, the characterisation of the Quaternary deposits emerge comparing the lithostratigraphic and the Standard Penetration Tests (SPT — ASTM, 2011), data (Table 2).

3.2. Geophysical investigations

Geophysical investigations were performed to a) correlate the point information derived from the boreholes; b) reconstruct the geometry of the gypsum rockhead; c) identify the presence of large voids; d) detect sinkholes with geomorphic expression; e) locate the buried "Alto Tagliamento" overthrust to determine the area where the gypsum is present (hanging-wall). The geophysical surveys were carried out mainly in the inhabited area, where the risk is higher, and where it was feasible to perform them.

Due to a high vertical and lateral variability of the geological and hydrogeological characteristics, no single geophysical technique alone could resolve the problem. Therefore, an investigation combining several methods was recorded to achieve a satisfactory geological model. The data were acquired using wave fields methods like Reflection seismic and Ground Penetrating Radar — GPR, (Fig. 3).

GPR surveys were conducted both in the village area and in the surroundings to image the possible shallow subsidence related to the deep dissolution features. The reflection seismic surveys were performed with two main objectives: 1) to obtain information at a large scale on the tectonic structures (L1), and 2) to gather detailed information to improve the borehole correlation in a highly inhomogeneous environment (L3).

The GPR profiles were collected using the ProEx Malå Geoscience GPR and the Zond-12 instrument developed by Radar System. Several shielded antennas were tested with frequencies between 250 and 800 MHz to obtain different resolution levels and penetration depths. The total length of the acquired profiles exceeds 1.5 km. Standard processing was used, which included DC (i.e. very low frequency components) removal, time drift correction, background removal, bandpass filtering, spherical divergence correction and exponential amplitude recovery, velocity analysis through diffraction hyperbola fitting, and depth conversion. Migration algorithms were also tested both to focus the scattered events and to reconstruct the actual dip of reflectors, but the very complex velocity field related to the presence of large vertical and especially lateral changes of the subsurface materials did not allow to obtain satisfactory imaging.

The seismic reflection survey was conducted in August 2012 along the L1 and L3 lines, 1090 and 231 m long, respectively (Fig. 3). Line L1 was acquired with a fixed-spread configuration, 5 m of trace interval and six vertical geophones (10 Hz natural frequency) per station, placed in a 2 m linear array. An IVI Minivib T-2500 operating with 2500 lbs peak force (two to four energizations per point), 14 s linear upsweep (in the 8–250 Hz frequency range) as a seismic source with a shot interval of 10 m was used. The recording parameters included a 1 ms sampling rate and 18 s of recording time. Vibroseis pilot signals were acquired and subsequently used (ground force) for the correlation. Line L3 was acquired with a fixed-spread configuration, 1 m of trace interval and a single 10 Hz vertical geophone, 0.5 ms sampling rate and 1.5 s of data length. Line L3 was shot with an accelerated weight drop to increase the resolution capability, with a shot interval of 1 m. The seismic data for this study were acquired by using a Summit DMT telemetric system. A shot-by-shot real-time quality control was performed during the entire seismic survey.

A standard data processing sequence was adopted. It included: editing, cross-correlation (only for non-impulsive sources), vertical stacking, geometry, first arrival picking, spherical divergence recovery, predictive deconvolution, frequency filtering, coherent noise muting, static correction, velocity analysis, Normal Move Out (NMO) correction, stacking and time-to-depth conversion.

Table 1
Main recorded past events in the Quinis area and in the surroundings.

Id number	Date of occurrence	Reactivation	Depth [m]	Lenght 1 [m]	Lenght 2 [m]	Shape
1	1962		10	15	30	Complex
2	1962	1965		7	7	Cylindrical
3	1963			15	20	Cylindrical
4	2nd Oct 1964		15	45	45	Cylindrical
5	5th Oct 1964		15	25	25	Cylindrical
6	1985	2012	3.5	4	4	Cylindrical
7	1985		0.2–0.3			

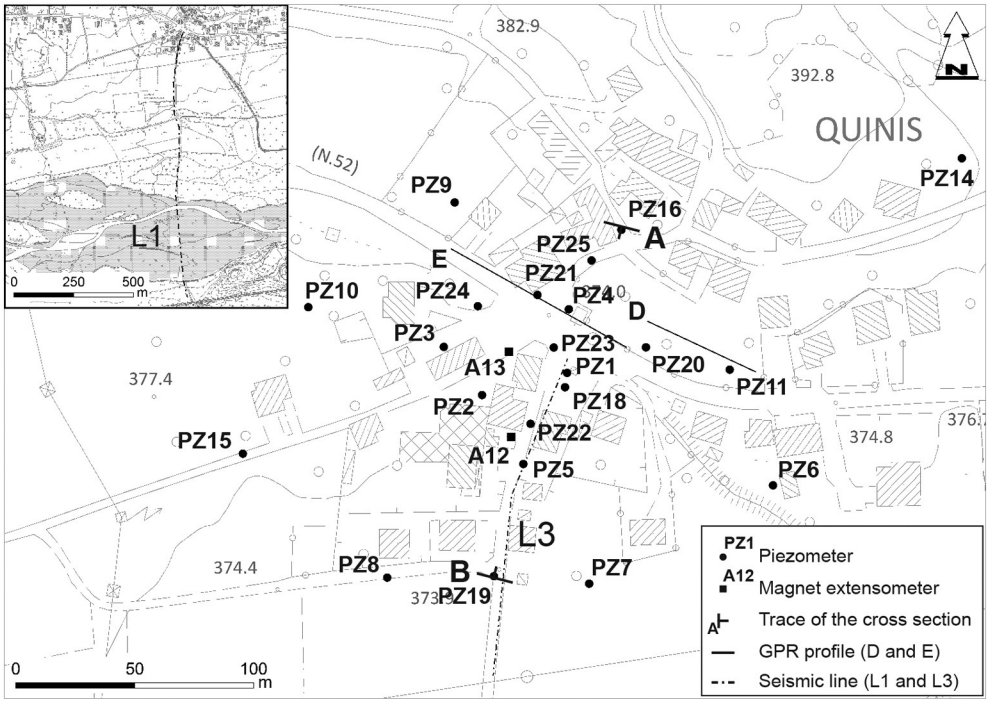

Fig. 3. Location map of the direct measurements (piezometers — PZ, magnet extensometers — A) and geophysical seismic sections L1, L3 and GPR (D, E). The figure only shows the location of the geophysical data described in the paper. A–B are the starting and ending points of the geo-stratigraphic section of Fig. 10.

In addition to the surface seismic data, a borehole was used to guide the data interpretation and to better convert the time-to-depth for the surface seismic data. In borehole PZ19, the Vertical Seismic Profiles (VSP) were acquired by using 3C wall-clamping borehole geophones (Huang and Wong, 2011) and hydrophone strings (Petronio and Poletto, 2010). An accelerated weight drop was used at different source points. The near-offset data were used to obtain a reliable seismic velocities profile while the offset VSP was used for imaging beneath and laterally away from the borehole.

3.3. Hydrogeological and geochemical investigations

Water monitoring was aimed at identifying the relation between the groundwater level fluctuations and the sinkhole activity, while the geochemical investigations allowed to characterize the waters and to identify the aquifer systems. Groundwater was monitored in 22 piezometers and in one spring (S1-Fornace spring) located on the northern hills (Fig. 1). Nine piezometers were equipped with CTD-Divers (conductivity, water level and temperature data-loggers), and 10 with TD-Divers (water level and temperature data-loggers). Both devices were manufactured by the Schlumberger company, and record the parameters every 30 min. The instruments measure the water level ranges with an accuracy of ±0.05% and a resolution of 0.02% of the measured value. Temperatures can be recorded in the range between −20 and 80 °C with an accuracy of ±0.1 °C and a resolution of 0.01 °C. Only CTD record the EC values (Electrical Conductivity). For the EC, the measured range is 0–120 mS/cm with an accuracy of ±1% and a resolution of 0.1 mS/cm.

The boreholes were drilled in different years (1982–2013), and only some of them reached the evaporitic bedrock. Screens were placed within the cover deposits and/or the bedrock reaching the aquifer.

Chemical and geochemical analyses were performed on 24 water points. The major ions were analysed (Na^+, K^+, Mg^{2+}, Ca^{2+}, F^-, Cl^-, NO_3^-, SO_4^{2-}, CO_3^{2-}) as well as oxygen ($\delta^{18}O$) and hydrogen (δD) isotopes (9 sampling campaigns between April 2012 and November 2013). The EC, pH and Eh were measured in situ with a portable CRISON MM26+ instrument, with an accuracy <0.1 °C for temperature, <1 mV for Eh and <0.01 for pH, with a resolution of 0.1 °C, 1 mV and 0.01, respectively. The Eh was referenced to the standard hydrogen electrode by its measurement against a ZoBell's solution (Nordstrom, 1977). To measure the EC, a portable instrument manufactured by WTW was used, which had an accuracy of 0.1 μS/cm and a resolution of ±0.5 °C (between 0 and 15 °C) and ±0.1 °C (between 15 and 35 °C). The alkalinity was measured by acidimetric titration using 0.1 N HCl, with a confidence of 5%. The total alkalinity was attributed to $HCO3^-$. The major constituents were obtained using a Dionex DX 120 ion chromatograph; $\delta^{18}O$ and δD measurements were conducted using the well-known CO_2/H_2 water equilibration technique (Epstein and Mayeda, 1953; Horita, 1988). The precision of the $\delta^{18}O$ and δD measurements was ±0.07‰ and ±0.7‰, respectively.

4. Results

The Quinis area is strongly influenced by anthropogenic activity. The centre of the village is crossed by an important State Road (S.S. 52) while just outside the centre an intense agricultural activity is present. All the sinkholes occurred through the years were filled by anthropogenic deposits soon after their formation. The depressions in the centre of the village or along the roads are partially covered by asphalt. This practice preclude identifying sinkholes on the basis of geomorphic criteria as the sinkholes described by Gortani (1965) (Fig. 2A), that are no longer visible. Therefore, it is necessary to apply different approaches to gain information about the buried sinkholes and the subsurface karst features.

4.1. Stratigraphic and geotechnical outcomes

The Quaternary deposits that cover the bedrock are characterized by heterogeneous sediments with a wide range of geotechnical properties. Analysing the available stratigraphies, it is very difficult to correlate the corresponding layers between neighbouring boreholes, but a visible change in the characteristics of the deposit is observed, with marked differences between the shallower part with more rounded and sub-

Table 2
Summary of the SPT and drilling results for each different borehole to characterize the bearing capacity of the deposit mantling the karst bedrock. D = depths below ground level [m]; SPT = number of blows or "N-value"; LBC = low bearing capacity; VLBC = Very Low Bearing Capacity (dropping corer −); CL = alternations of cemented layers; void.

Boreholes													Bedrock [m] b.g.l.
PZ1	D [m]	−3	−6,1	−9	−13,5	−18							−18,8
	n SPT	24–13–23	5–6–9	8–7–9	3–3–5	6–1–0							
PZ2	D [m]	−3,2	−6	−9,5	−12	−15	−16,5 to −17	−17	−18,6	−20	−20,5		−23,3
	n SPT	4–6–6	3–3–5	7–11–7	4–13–12	7–8–7	VLBC	4–7–10	12–14–12	5–6–8	8–12–9		
PZ3	D [m]	−3	−6	−7,3	−12	−15	−18	−21	−24	−23,8 to −27	−29 to −29,8		−27,5
	n SPT	1–5–6	8–refuse	5–8–13	3–12–13	5–17–20	7–12–16	4–5–7	1–1–1	VLBC	Void		
PZ4	D [m]	−3	−3,50 to −3,80	−6	−9	−12	−15						−16,9
	n SPT	Refuse	LBC	6–8–7	3–5–4	1–1–2	7–8–9						
PZ5	D [m]	−3	−6	−9	−12	−15	−18	−21	−22,5 to −28,3	−28,3			−28,7
	n SPT	4–3–5	4–2–2	5–9–8	7–18–11	6–12–15	5–6–5	3–4–6	VLBC	3–6			
PZ6	D [m]	−24,5 to −25,5											−35,8
		LBC											
PZ7	D [m]	−20 to −35	−35 to −39,7										−39,7
		CL	LBC										
PZ8	D [m]	−20 to −27											−39,7
		CL											
PZ9	D [m]	−4,5 to −15	−35 to −37										−37
		CL	LBC										
PZ10	D [m]	−27 to −29	−29 to −30	−30 to −31	−31,5 to −32								−31
		LBC	Void	LBC	Void								
PZ11	D [m]	−3	−4,5	−6	−9	−12	−16,5						−18,9
	n SPT	4–7–6	3–4–4	7–5–5	4–3–6	6–7–8	8–9–10						
A12	D [m]	−2,8	−4,5	−6	−7,5	−12	−15	−18	−22,5 to −30,5				−30,5
	n SPT	10–18–17	2–2–3	5–6–5	10–5–4	7–4–6	9–12–14	13–17–12	LBC				
A13	D [m]	−2,9	−6	−12	−15	−18,5 to −20							−28,7
	n SPT	1–3–4	4–6–8	3–5–8	7–10–15	LBC							
PZ14	D [m]	−2,9	−6	−9	−12	−15	−6,30 to −18,4						−20,4
	n SPT	3–4–5	3–2–3	1–2–8	4–2–2	1–1–3	LBC						
PZ15	D [m]	−3	−4,5	−6	−7,5	−9	−10,5	−12	−13,5	−15	−18	−21	−23
	n SPT	17–10–6	1–2–2	2–3–5	2–4–4	2–3–3	5–7–5	4–7–13	7–8–11	8–29–refused	5–11–9	6–10–18	
PZ16	D [m]	−2,8											−4,6
	n SPT	2–3–2											
PZ18	D [m]	−3	−4,5	−6	−7,5	−9	−10,5	−12	−13,5	−15	−18		−19,5
	n SPT	4–4–3	9–6–4	4–5–7	6–6–8	3–3–2	10–7–5	4–4–6	7–8–11	8–6–5	5–7–8		
PZ19	D [m]	−37 to −40											−51,7
	n SPT	LBC											
PZ20	D [m]	−5,8											−11,7
	n SPT	6–5–3											
PZ21	D [m]	−5,8											−13,4
	n SPT	2–6–10											
PZ22	D [m]	−7,2	−10,2	−22,7	−18,6 to −36,8								−37,8
	n SPT	9–11–11	1–3–6	1–0–0	LBC								
PZ23	D [m]	−5,4 to −5,5	−7,3	−16,7 to −19,3									−19,3
	n SPT	CL	13–14–14	LBC									
PZ24	D [m]	−5,8	−8,8	−12	−16,5	−19,5	−22,7	−22,7 to −24,4	−25				−26,7
	n SPT	2–5–7	3–7–11	3–8–12	8–18–13	11–15–17	3–8–4	LBC	1–0–0				
PZ25	D [m]	−2,7											−3,7
	n SPT	3–1–2											

rounded clasts, and the deeper part, where angular clasts are present, indicating little or no transport before the deposition. The SPT values, compared with the observations made during drilling, often reveal very low mechanical resistance (Table 2). An anomalous decrease in the geotechnical quality at increasing depths has frequently been observed. This trend is clearer in the centre of the village (PZ1, PZ3, PZ4, PZ5, PZ22, PZ23 and PZ24) and in the northern sector of Quinis (PZ14). It is remarkable that PZ1, PZ3, PZ22 and PZ24 at depths of around 20–25 m show SPT values close or equal to zero (Fig. 3 and Table 2).

The decrease in mechanical strength is primarily associated with the lithological transition between the Quaternary deposits and the evaporitic bedrock. The lower SPT values were recorded in correspondence with clay and clayey-silt lenses. In some of the boreholes, small voids were also intercepted: in PZ3 between 29 and 29.8 m depth, and in PZ10 at 29–30 m and 31.5–32 m below the ground level (Table 2). In contrast, south of Quinis, cemented layers of gravels are present above the low bearing capacity units (Table 2 — CL). Within this framework, magnet extensometers are a very useful tool to monitor deep vertical movements (Fig. 3). They were installed in the boreholes nearby the most damaged houses and where it was logistically possible. Since May 2011, the magnet extensometer in borehole A12 indicates stability. On the other hand, the magnet extensometer in A13 shows a differentiated behaviour between its shallow (0–10 m), intermediate (10–16 m) and deepest (17–32 m) parts. In the shallower section, no meaningful movements were recorded. Conversely, the central part shows a stable behaviour until 2013 and then a progressive lowering. The deepest part is lowering since June 2011 with values varying according to the water table fluctuations (Fig. 4): the maximum differential values are recorded in correspondence of a quick water table lowering, 119 mm between April and May 2014 and 126 mm within May and August 2014. When the water table is high, the lowering movements do not exceed 40 mm. An evidence of the ground lowering effect can be plainly seen in Fig. 4B and C where the same point has been pictured in two different moments (Fig. 4B — 12.02.2014 and C — 30.09.2014). Suddenly after its occurrence, the forming hole was promptly filled with new asphalt.

During the first year of monitoring, the maximum lowering has been recorded at a depth between 27.8 and 29.6 m, in correspondence of the weathered evaporitic bedrock. From September 2013, and especially in 2014, the above layers (20–26.8 m) recorded the maximum lowering. This monitoring activity suggests the presence of a progressive subsidence that from the deeper layers progressively involve the upper ones.

4.2. Geophysics

In order to extend 1D information obtained by boreholes data into 2D, geophysical techniques were applied to investigate the Quaternary deposits and the karstified evaporitic bedrock. In zones characterised by high building density as in the Quinis area, designing the layout of the geophysical surveys is often difficult due to the presence of multiple limitations (human structures, artefacts, noises, etc.). As an example, GPR profiles acquired with 300 MHz antennas in a car parking area to the East (D on Fig. 5) reveal the presence of a depocentre (S1), but the overall quality of the data is quite low due to the presence of the reverberations (R) and diffraction hyperbolas that are primarily related to

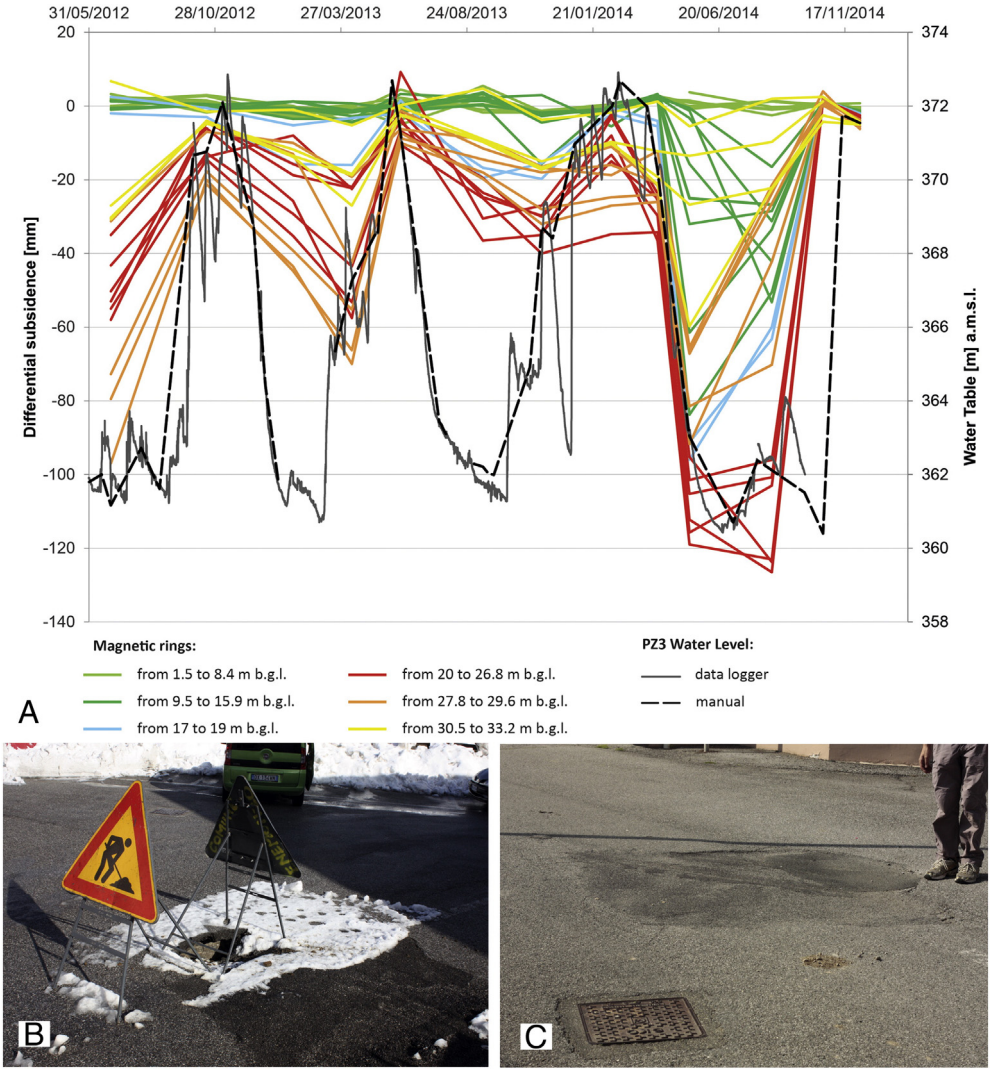

Fig. 4. A) Measurements comparison between groundwater level (PZ3) and the lowering of the magnet extensometer (A13). In black the water table fluctuations (continuous line shows data coming from data-logger device; dotted line from manual measurements). Each coloured line corresponds to a specific magnetic ring. Coloured dots represent the lowering of each single ring between two measuring surveys (differential lowering). Hole evidences on 12.02.2014 B) and after few months, 30.09.2014 C).

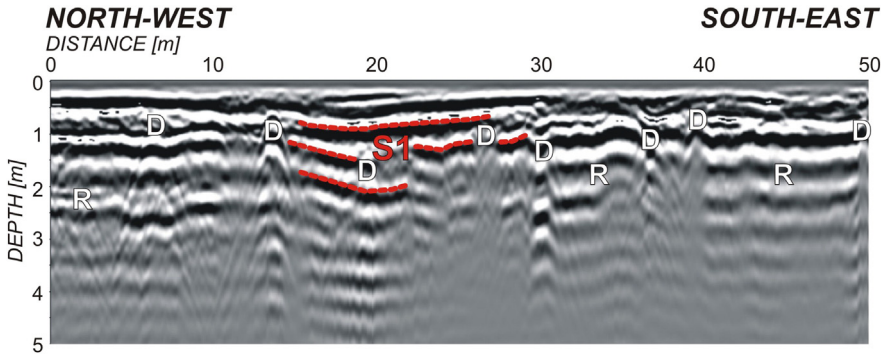

Fig. 5. Example of GPR profile (Fig. 3) acquired with 300 MHZ antennas showing a synform attributable to a buried sinkhole (*S1*), partially masked by scattering objects (*D*) and coherent noises, such as reverberations (R).

shallow pipes and buried cables that obscure the natural reflectors. On the other hand, seismic methods are strongly limited by logistical problems and by heterogeneous soil that attenuates the signal and prevents the seismic source's repeatability. Despite all of these limitations and difficulties, the direct and indirect investigations that were applied are widely recognised as suitable techniques to characterise cover deposits and the rockhead in karst areas.

In the present research a GPR survey with antennas of different frequencies was performed (Fig. 6), allowing to image the subsurface with high resolution, even if the maximum depth of penetration does not exceed few metres, even using relative low frequency antennas (Fig. 6A).

The profiles obtained with the different antennas show sagging structures with cumulative indicative of progressive subsidence. In fact, the imaged reflectors show increasing dips with depth, highlighting some depocentres (d1, d2, d3 and d4 on Fig. 6) and abrupt lateral variations (dotted lines). It is interesting to note that at least the shallowest folded reflection could be interpreted as the deformed base of the asphalt, whereas the deepest sagged horizons can be related to both man-made fillings and natural deposits. This is a useful information that is actually very difficult to obtain by any direct technique in an urban area.

The GPR only investigates the shallower layers and so additional techniques were used to explore the overburden bedrock contact. Deep seismic investigation defined the top of the evaporites and their southern edge beneath the Tagliamento River valley.

The N-dipping “Alto Tagliamento” overthrust, which separates the evaporites from the Monticello dolostones, is believed to be buried below the alluvium of the Tagliamento River deposits. The location of this contact has relevant implications from the sinkhole hazard perspective. The location and the acquisition parameters for the L1 seismic line were selected for a deep investigation to reach the target structure.

As evidenced by the L1 seismic section (Fig. 7) that crosses the Tagliamento valley in a north–south direction (see location in Fig. 3), the southernmost sector is characterised by strong reflected signals corresponding to the Quinis village (the northern sector) and the lack of consistency in the wavelet's character and reflection continuity is indicative of a chaotic area where it is extremely difficult to identify any type of structure. The abrupt interruption of the reflections and the strong

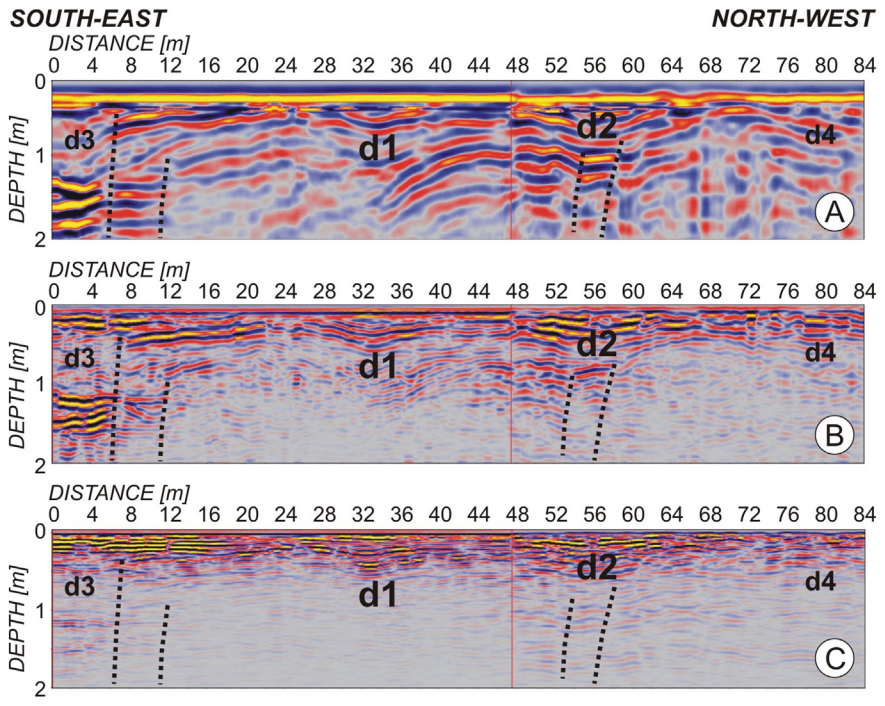

Fig. 6. Processed and interpreted GPR profiles acquired with different antennas: A) 250 MHz; B) 500 MHz; C) 800 MHz (E on Fig. 3). d1, d2, d3 and d4 highlight the centre of four subsidence zones, while the dotted lines mark main lateral variations in the reflections. The red vertical segments on the GPR profiles depict the transition between two different types of road pavement.

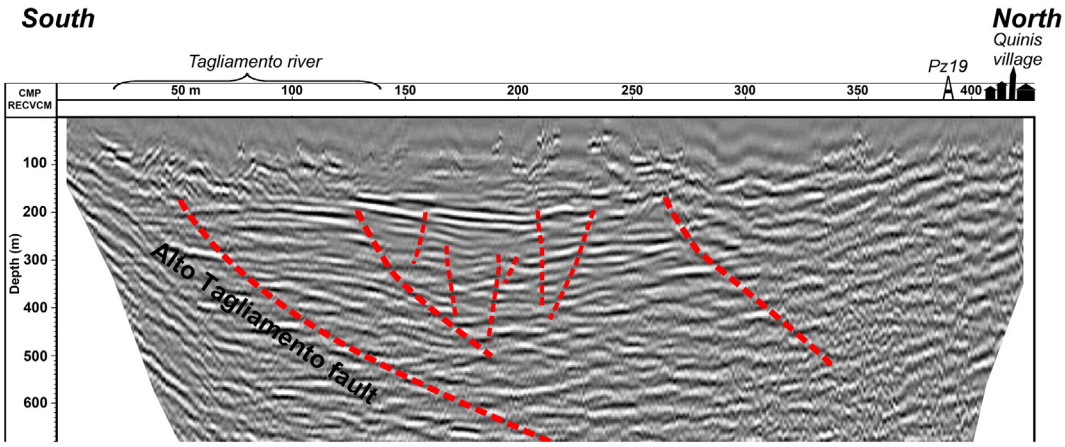

Fig. 7. Reflection seismic Line L1 — Dashed lines correspond to the interpreted faults. Depth conversion was obtained by using a constant velocity equal to 2000 m/s. In the southern limit of the section artefacts related to border effects are apparent.

lateral variation in the seismic signals allow the interpretation of the buried "Alto Tagliamento" thrust fault.

L1 results are obviously not enough detailed in the shallower horizons to understand the infrastructure instability causes, and a new acquisition was performed with different resolution characteristics. A high resolution seismic line (L3, Fig. 8) was acquired along the northern sector of line L1 to laterally extend the 1D information derived from borehole data (Fig. 3). The position of the rockhead of the evaporitic bedrock was calibrated using the boreholes. The geometry of the evaporite bedrock is very articulated, with a sequence of highs and depressions characterised by steep slopes. This complex buried geometry is also confirmed by offset VSP data that show downgoing signals with anomalous arrival times.

4.3. Hydrogeology

The bedrock morphology with its depressions affects the groundwater flow conditioned by the extreme heterogeneity of the Quaternary deposits and to the different karstification degree of the evaporitic bedrock. As evidenced by boreholes and geophysical data, the Quaternary aquifer system is very complex. The presence of clayey and clayey-silt layers with limited lateral extent generates local perched aquifers as recognised in piezometers PZ3, PZ5 and PZ24.

Seasonal water level fluctuations are large, with oscillations between 6 and 32 m. The maximum values related to the snowmelt and rainfall are recorded during Spring and late Autumn, respectively, and the minimum levels are recorded during Winter (January–March) and summertime (July–August), when some of the piezometers (PZ4, PZ5 and PZ11) dry out (Winter 2012).

In the piezometers located in the southern side of Quinis (PZ7 and PZ8), the water table fluctuations are wider. Sometimes the rise of the water table is so fast that the piezometers top cover starts to stir due to the difference in the air pressure. These circumstances indicate that the water table has a rapid response to rainfall. The main rainfall event occurred within the monitoring period recorded 248 mm of rain in 56 h (24–26 December 2013). In such occasion, the water table raised from 1.16 m (in correspondence of PZ14) up to 11.26 m (in PZ7). The rising calculated velocities ranges approximately between 5 (PZ14) and 40 cm/h (PZ7).

From a geochemical point of view, all the analysed waters can be classified as calcium-sulphate, but present a different mineralization. The monitoring field EC and Eh measurement allowed to identify waters with different characteristics. Low EC values are typical of the piezometers having the screens in alluvial sediments (EC < 1 mS/cm), while very high EC values are recorded in piezometers with screens in the evaporitic bedrock (EC > 2 mS/cm). The Eh shows significant fluctuations, but negative values are related only to the piezometers with screens in the bedrock.

The water type difference is confirmed also through the $\delta^{18}O$ isotopic analyses conducted on rainfall and groundwaters. The rainfall values were available since 2006 (DMG, 2014), in which $\delta^{18}O$ shows a sinusoidal behaviour related to the seasonality and the temperature, with values between −3.5‰ and −15.4‰. The same variability is recorded for the groundwaters, with more negative values during the spring time, when the snowmelt occurs (−12.37‰ PZ18c min value) and less negative values during late summer time (−6.93‰ PZ11 max value). The more negative values were recorded in the piezometers reaching the evaporitic bedrock. An example of this situation can be seen in correspondence of PZ18, where three piezometers are set with screens at different depths (18a: screen between 6 and 12 m b.g.l., 18b: screen between 19 and 25 m b.g.l., 18c: screen between 28 and 40 m b.g.l.). Groundwaters present in the Quaternary deposits (18a) has values that

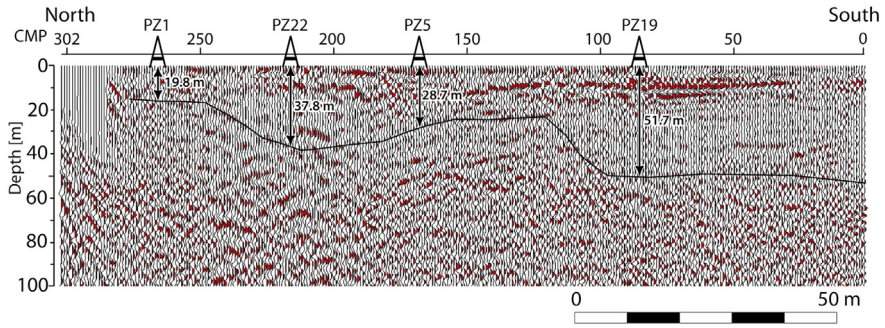

Fig. 8. Reflection seismic Line L3. Black thick lines indicate the top of the evaporitic bedrock calibrated with borehole data from PZ1, PZ22, PZ5 and PZ19. Time to depth conversion was carried out by using a constant velocity equal to 1000 m/s.

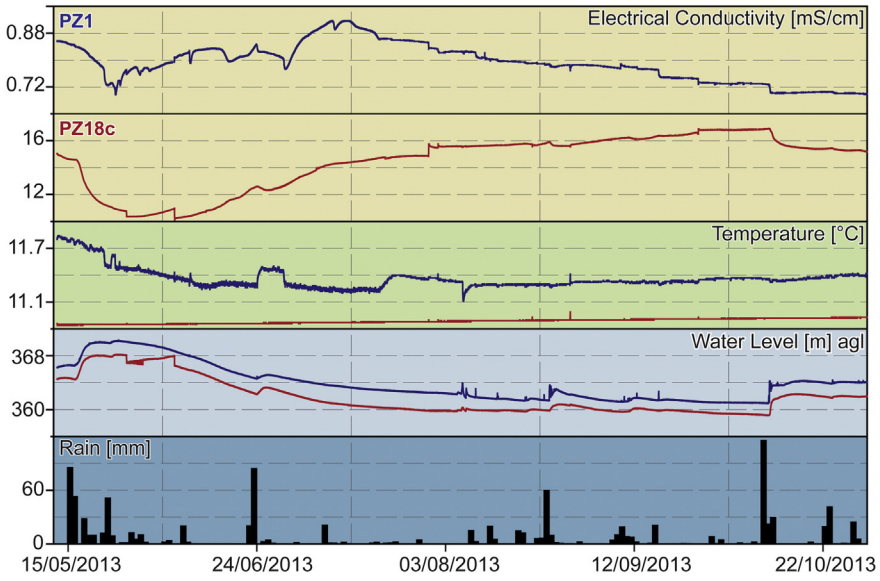

Fig. 9. Comparison of rainfalls [mm], water levels [mm a.s.l.], temperature [°C] and electrical conductivity [mS/cm] between piezometers PZ1 and PZ18c in relation to the rainfall data.

range between −8.77‰ and −8.81‰ and a mean of −8.79‰; the ones present in the evaporitic rockhead (18b) has values that range between −8.2‰ and −9.81‰ and a mean of −9.1‰. Finally, the ones coming from the evaporitic bedrock (18c) have values ranging between −8.68‰ and −12.37‰ and a mean of −9.28‰. These data show waters that have different recharge areas and that are poorly connected. What highlighted above can be clearly seen also from the data recorded by the data logger devices in PZ1 (screen only in the Quaternary deposits: 7–19 m b.g.l.) and PZ18c (screen only in the evaporitic bedrock), (Fig. 9). The two piezometers were drilled at a small linear distance of only 8 m, but their recorded data are quite different. The water level in PZ18c is constantly 2 m lower than in PZ1, the EC value is one order of magnitude higher than in PZ1 and the temperature is always lower and more stable than PZ1.

The different mineralization degree, the different isotopic values and the different water levels but with similar fluctuations highlight the poor connection existing between the groundwaters recognized in the Quaternary deposits and the ones flowing in the karstified evaporitic bedrock suggesting the presence of two aquifers: an unconfined and a semi-confined.

5. Discussion and conclusions

In a complex geological framework as Quinis, the multidisciplinary approach adopted is the best way to identify and understand the occurring phenomena. The data interpretation allowed to reconstruct the rockhead morphology and the hydrogeological behaviour of the groundwaters. The integration of all the acquired data get to a complete overview of the vulnerability of the area.

Taking advantage of the geomorphological and geophysical investigations, first of all, the sinkholes were identified and classified. Globally, in the Enemonzo and Quinis area, informations concerning 64 sinkholes were collected: the most part is represented by cover collapse sinkholes (38), cover suffosion sinkholes are less frequent (26). In the inhabited zones, the identification of the subsiding areas, is more difficult due to the presence of the anthropogenic structures tending to mask any effect on the territory. In this framework, the geophysical techniques (non-invasive) have proven to be a helpful tool in the instabilities mapping. In fact, reflection seismics allowed an approximated identification of the rockhead due to the absence of a sharp transition between the deposits and the evaporite bedrock and GPR technique was particularly effective to image the shallowest levels. Most part of the layers identified can be

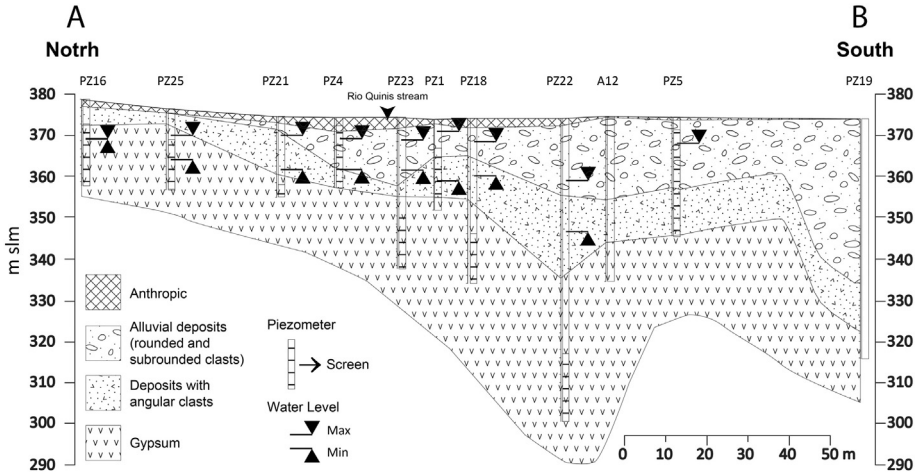

Fig. 10. Cross-section of the study area based on borehole stratigraphy and seismic data (line L3). Piezometers with screens at different depths, as well as water table maximum and minimum levels indicate the presence of different aquifers: one unconfined and one semiconfined.

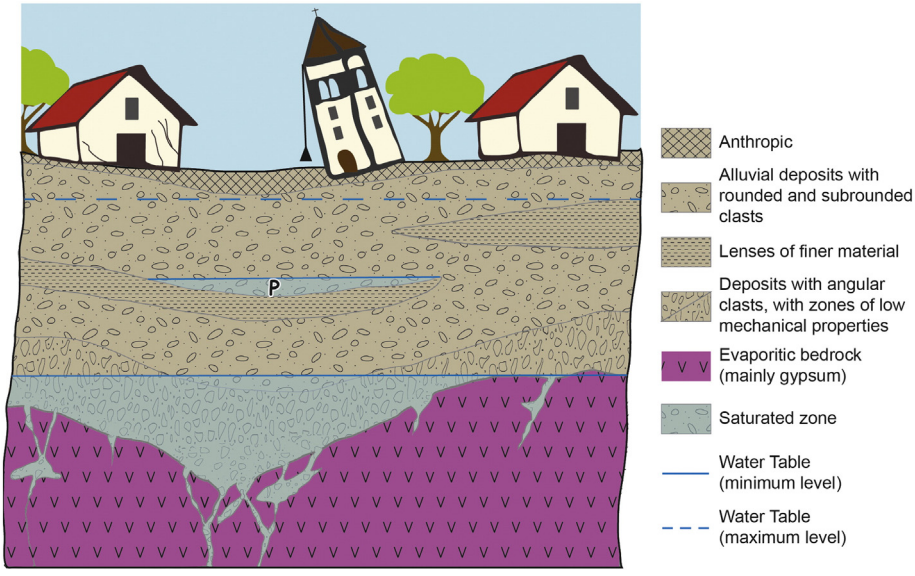

Fig. 11. Conceptual model of the Quinis subsoil obtained integrating borehole, geophysical, hydrogeological and geotechnical data. The sagging–suffosion surface morphologies correspond to the subsidence features on the karstified head-rock. Damages are represented on the infrastructures. Down-wash processes occur through the karst fissures.

correlated to human activities (asphalt, road basements), realized within the years, often to mitigate the effects of the subsidence itself. Their morphology, entirely similar to a geological depocenter (even if a totally different scale), demonstrates that the actual movements persisted over time. These phenomena, although detectable with the GPR, only up to a limited depth, suggest the presence of deeper and generalized movements. The punctual information derived from the drilled boreholes and the magnet extensometer monitoring, were extended laterally by the geophysical investigations, making thus possible to reconstruct the bedrock morphology beneath the Quinis village (Fig. 10).

In the centre of the village where the bell tower affected by subsidence is located, there is a high in the rockhead (19–25 m b.g.l.) surrounded by steep slopes deepening towards S, E and W (reaching 35–40 m b.g.l.). In the proximity of the bedrock high, four depressions are recognised. They are located between: 1) PZ23, PZ21 and PZ20, 2) PZ3 and PZ23, 3) PZ18 and PZ12, and 4) PZ7 and PZ8.

To geotechnically characterise the Quaternary deposits mantling the bedrock, boreholes and SPT tests were performed. The results indicate the presence of low bearing capacity deposits at different depths and the presence of voids in all of the stratigraphic units. Lower values are mainly recorded in the Quaternary deposits especially at the contact with the evaporitic unit, probably related to the presence of soft karstic residual and suffosion zones with washing-out points. In the last fifty years, this washing-out process was magnified by the construction of the dam located 15 km upstream the study area on the Tagliamento River, the water table depth lowered and the fluctuations amplified. A lowering in the water table, up to 4 m, was recorded in a piezometer located approximately 4 km SE of the study area. This caused the loss of hydrostatic support and an acceleration of the washing-out processes. Just after this period, the most important cover collapse sinkholes (Fig. 2) were recorded (Gortani, 1965). In addition, the occurrence of always more intense rainfall events generates more extreme and faster answer in the hydrogeological system (Groisman et al., 2005; Cicogna et al., 2012).

Even if not completely clear at first, the distribution of the subsidence phenomena presents a spatial pattern. The largest known cover collapse sinkholes are aligned along a NW-SE belt, extension of the fault that in the northern area corresponds to the Rio Quinis riverbed (Fig. 1), which seems to be related to the projection of the fault controlling the entire structure of the Alto Tagliamento valley.

Furthermore, there seems to be a correlation between the secondary drainage network and the distribution of sinkholes. The majority of the streams show an influent character especially in the proximity of the alluvial fans. Here, the downward vadose groundwater flow, combined with the low thickness of the Quaternary deposits, favour the sinkhole occurrence.

Two different genetic processes were recognised. In the Quinis village area the integration of borehole, geophysical, hydrogeological and geotechnical data suggests a, slow surface subsidence consisting of a passive sagging of the cover linked to the washing-out of debris through solutional fissures and pipes in all the bedrock, thus generating cover sagging and suffosion sinkholes (Fig. 11). These are long-lasting phenomena, documented since the 19th century (Marinelli, 1898), whereas there is no information in living memory of cover collapse sinkholes in the inhabited area. As defined by the extensometer movements (A13), the subsiding phenomena are not regular, but are amplified in the low flows when a quick lowering of the water table is observed. On the contrary, the movements are smaller when the water level is high (Fig. 4).

The situation is quite different in the southern sector of Quinis, where the influence of the Tagliamento River is greater and where collapses occur in the Quaternary deposits due to the failure of the compact layers within the deposits or within the karstified bedrock where cave roof collapses may occur (Fig. 2). So far, it is impossible to predict the occurrence of any future sinkhole. However the hazard level may vary within the location according to the type of the past recorded events. On the southern side of the Quinis area, close to the Tagliamento riverbed, the hazard seems to be higher due to the greater presence of recorded collapse events.

Situations similar to that in Quinis are present in the entire Alta Val Tagliamento valley where evaporites crop out, or are mantled by Quaternary deposits. For this reason, the results obtained in the presented study and the methodological approach adopted can be extended to other areas having similar geological and hydrogeological characteristics.

Acknowledgements

The Authors would like to thank Francesca Slejko and Barbara Stenni for the geochemical analyses; the functionaries and the residents of the Enemonzo Municipality for their priceless information and help. The study was funded by the Municipality of Enemonzo and by the Geological Survey of the Friuli Venezia Giulia Region in the framework of Prot.no. 412/09/11/2011.

References

ASTM Standard D1586-11, 2011. Standard Test Method for Standard Penetration Test (SPT) and Split-Barrel Sampling of Soils. ASTM International, West Conshohocken, PA http://dx.doi.org/10.1520/D1586-11 (www.astm.org, website visited in Maj 2014).

Bechstadt, T., Schweizer, T., 1991. The carbonate—clastic cycles of the East-Alpine Raibl group: result of third-order sea-level fluctuations in the Carnian. Sediment. Geol. 70, 241–270.

Beck, B.F., 2004. Soil piping and sinkhole failures. In: White, W.B. (Ed.), Encyclopedia Of Caves. Elsevier, New York, pp. 523–528.

Benson, R.C., Kaufmann, R.D., 2001. Characterization of a highway sinkhole within the gypsum karst of Michigan. In: Beck, B.F., Herring, J.G. (Eds.), Geotechnical And Environmental Applications Of Karst Geology And Hydrology. Balkema, Lisse, pp. 103–112.

Brinkmann, R., Wilson, K., Elko, N., Seale, L.D., Florea, L., Vacher, L., 2007. Sinkhole distribution based on pre-development mapping in urbanized Pinellas County, Florida, USA. In: Parise, M., Gunn, J. (Eds.), Natural and Anthropogenic Hazards in Karst Areas: Recognition, Analysis and Mitigation. Geol. Soc. London, Special Pub. 279, pp. 5–11.

Brinkmann, R., Parise, M., Dye, D., 2008. Sinkhole distribution in a rapidly developing urban environment: Hillsborough County, Tampa Bay area, Florida. Eng. Geol. 99, 169–184.

Brusca, C., Gaetani, M., Jadoul, F., Viel, G., 1982. Paleogeografia ladinico-carnica e metallogenesi del sudalpino. Mem. Soc. Geol. Ital. 22, 65–82.

Burelli, G., Cleva, S., Cucchi, F., Oberti di Valnera, S., 2004. Stato di evoluzione di sinkholes in alcune aree montane del Friuli Venezia Giulia. 1° Seminario Stato dell'arte sullo studio dei fenomeni di sinkholes. APAT, Roma, pp. 159–170.

Butler, D.K., 1984. Microgravimetric and gravity gradient techniques for the detection of subsurface cavities. Geophysics 49, 1084–1096.

Calligaris, C., Zini, L., Cucchi, F., Stefanelli, S., 2009. Gypsum's role in the Friuli Venezia Giulia Sinkholes. Proceedings of the 2°Seminario "I sinkholes: gli sprofondamenti catastrofici nell'ambiente naturale ed in quello antropizzato". ISPRA, Roma, pp. 213–221.

Cardarelli, E., Cercato, M., Cerreto, A., Di Filippo, G., 2010. Electrical resistivity and seismic refraction tomography to detect buried cavities. Geophys. Prospect. 58, 685–695.

Cardarelli, E., Cercato, M., De Donno, G., Di Filippo, G., 2014. Detection and imaging of piping sinkholes by integrated geophysical methods. Near Surf. Geophys. 12, 439–450.

Carulli, G.B., 2006. Carta geologica del Friuli Venezia Giulia alla scala 1:150.000 e Note Illustrative. SELCA (Eds.), Firenze.

Cicogna, A., Gani, M., Micheletti, S., 2012. Cambiamenti climatici. Rapporto Sullo Stato dell'Ambiente, ARPA FVG, Forum. Editrice Universitaria, Udine.

Cooper, A.H., Calow, R., 1997. Gypsum Geohazards: their impact on development-project. Technical Report, WC/97/17. British Geological Survey, Nottingham.

Cooper, A.H., Calow, R.C., 1998. Avoiding gypsum geohazards: guidance for planning and construction. Technical Report, WC/98/5. British Geological Survey, Nottingham.

Cooper, A.H., Waltham, A.C., 1999. Subsidence caused by gypsum dissolution at Ripon, North Yorkshire. Q. J. Eng. Geol. 32, 305–310.

Cucchi, F., Forti, P., 1993. Dissoluzione sottocutanea nei gessi: analisi e considerazioni. Proceedings of Atti Congresso Naz. Speleol. Udine 1990 1, pp. 89–100.

Cucchi, F., Piano, C., 2002. Ipercarsismo superficiale e sepolto nelle evaporiti del Friuli-Venezia-Giulia. Proceedings of Le voragini catastrofiche, un nuovo problema per la Toscana. Edizioni Regione Toscana, Grosseto, pp. 35–41.

Cucchi, F., Forti, P., Ulcigrai, F., 1994. Znizevanje krskega povrsja zaradi korozije (Valori di abbassamento per dissoluzione di superfici carsiche). Acta Carsologica 23, 55–61.

Dahm, T., Kühn, D., Ohrnberger, M., Kröger, J., Wiederhold, H., Reuther, C., Dehghani, A., Scherbaum, F., 2010. Combining geophysical data sets to study the dynamics of shallow evaporates in urban environments. Geophys. Int. J. 181–193.

Delle Rose, M., Leucci, G., 2010. Towards an integrated approach for characterization of sinkhole hazards in urban environments: the unstable coastal site of Casalabate, Lecce, Italy. J. Geophys. Eng. 7, 143–154.

DMG, 2014. Elaborazione del modello idrogeologico del sottosuolo e definizione della dinamica del dissesto che coinvolge l'area su cui sorge l'abitato di Quinis. Technical report. Università degli Studi di, Trieste, Italy.

Dobecki, T.L., Upchurch, S.B., 2006. Geophysical applications to detect sinkholes and ground subsidence. Lead. Edge 25, 336–341.

Dreybrodt, W., Eisenlohr, L., 2000. Limestones dissolution rates in karst environments. In: Klimchouk, A.B., Ford, D.C., Palmer, A.N., Dreybrodt, W. (Eds.), Speleogenesis: Evolutions In Karst Aquifers. National Speleological Society, Huntsville, pp. 136–148.

Epstein, S., Mayeda, T.K., 1953. Variations of ^{18}O of waters from natural sources. Geochim. Cosmochim. Acta 4, 213–224.

Ercoli, M., Pauselli, C., Frigeri, A., Forte, E., Federico, C., 2013. Geophysical paleoseismology through high-resolution GPR data: a case of shallow faulting imaging in Central Italy. J. Appl. Geophys. 90, 27–40.

Ezersky, M., 2008. Geoelectric structure of the Ein Gedi sinkhole occurrence site at the Dead Sea shore in Israel. J. Appl. Geophys. 64, 56–69.

Floreani, P., Jaiza, G., 1980. Ricerca geologica per la localizzazione delle aree non soggette a fenomeni di sprofondamento nel commune di Enemonzo. Technical report, Comune di Enemonzo (UD).

Ford, D., Williams, P., 2007. Karst Hydrogeology And Geomorphology. Wiley & Sons Ltd, West Sussex, England.

Forth, R.A., Butcher, D., Senior, R., 1999. Hazard mapping of karst along the coast of the Algarve, Portugal. Eng. Geol. 52, 67–74.

Furlani, S., Cucchi, F., Forti, F., Rossi, A., 2009. Comparison between coastal and inland karst limestone lowering rates in the northeastern Adriatic Region (Italy and Croatia). Geomorphology 104 (1), 73–81.

Galve, J.P., Gutiérrez, F., Lucha, P., Bonachea, J., Remondo, J., Cendrero, J., Gutiérrez, M., Gimeno, M.J., Pardo, G., Sánchez, J.A., 2009a. Sinkholes in the salt-bearing evaporitic karst of the Ebro River valley upstream of Zaragoza city (NE Spain). Geomorphological mapping and analysis as a basis for risk management. Geomorphology 108, 145–158.

Galve, J.P., Gutiérrez, F., Remando, J., Bonachea, J., Lucha, P., Cendrero, A., 2009b. Evaluating and comparing methods of sinkhole susceptibility mapping in the Ebro Valley evaporite karst (NE Spain). Geomorphology 111, 160–172.

Gortani, M., 1965. Doline alluvionali in Carnia. Mondo Sotterraneo. pp. 14–20.

Grandjean, G., Leparoux, D., 2004. The potential of seismic methods for detecting cavities and buried objects: experimentation at a test site. J. Appl. Geophys. 56, 93–106.

Groisman, P.Y., Knight, R.W., Easterling, D.R., Karl, T.R., Hegerl, G.C., Razuvaev, V.N., 2005. Trends in intense precipitation in the climate record. J. Clim. 18 (9), 1326–1350.

Guerrero, J., Gutiérrez, F., Lucha, P., 2004. Paleosubsidence and active subsidence due to evaporite dissolution in Zaragoza city area (Huerva River valley, NE Spain). Processes, spatial distribution and protection measures for linear infrastructures. Eng. Geol. 72, 309–329.

Gutiérrez, F., Cooper, A.H., 2002. Evaporite dissolution subsidence in the historical city of Calatayud, Spain: damage appraisal and prevention. Nat. Hazards 25, 259–288.

Gutiérrez, F., Cooper, A.H., Johnson, K.S., 2008. Identification, prediction and mitigation of sinkhole hazards in evaporite karst areas. Environ. Geol. 53, 1007–1022.

Gutiérrez, F., Galve, J.P., Lucha, P., Bonachea, J., Jordà, R., Jordà, L., 2009. Investigation of a large collapse sinkhole affecting a multi-storey building by means of geophysics and the trenching technique (Zaragoza city, NE Spain). Environ. Geol. 58, 1107–1122.

Gutiérrez, F., Galve, J.P., Lucha, P., Castañeda, C., Bonachea, J., Guerrero, J., 2011. Integrating geomorphological mapping, trenching, InSAR and GPR for the identification and characterization of sinkholes: a review and application in the mantled evaporite karst of the Ebro Valley (NE Spain). Geomorphology 134, 144–156.

Gutiérrez, F., Parise, M., De Waele, J., Jourde, H., 2014. A review on natural and human-induced geohazards and impacts in karst. Earth-Sci. Rev. 138, 61–88.

Horita, J., 1988. Hydrogen isotope analysis of natural waters using an H_2–water equilibration method: a special implication to brines. Chem. Geol. Isot. Geosci. Section 72, 89–94.

Huang, J., Wong, J., 2011. Integrated well log, VSP, and surface seismic analysis of near-surface glacial sediments: Red Lodge, Montana. SEG Technical Program Expanded Abstractspp. 526–530.

Iovine, G., Parise, M., Trocino, A., 2010. Breakdown mechanisms in gypsum caves of southern Italy, and the related effects at the surface. Z. Geomorphol. 54 (Suppl. 2), 153–178.

Jardani, A., Revil, A., Santos, F., Fauchard, C., Dupont, J.P., 2007. Detection of referential infiltration pathways in sinkholes using joint inversion of self-potential and EM-34 conductivity data. Geophys. Prospect. 55, 749–760.

Jeschke, A., Vosbeck, K., Dreybrodt, W., 2001. Surface controlled dissolution rates of gypsum in aqueous solutions exhibit nonlinear dissolution kinetics. Geochim. Cosmochim. Acta 65, 27–34.

Kaufmann, Y., Quinif, O., 2002. Geohazard map of cover-collapse sinkholes in the "Tournaisis" area southern Belgium. Eng. Geol. 65, 117–124.

Kaufmann, G., Romanov, D., Nielbock, R., 2011. Cave detection using multiple geophysical methods: Unicorn cave, Harz Mountains, Germany. Geophysics 76 (3), B71–B77.

Klimchouk, A., Lowe, D., Cooper, A., Sauro, U., 1996. Gypsum karst of the world. Int. J. Speleol. 25 (3–4), 1–307.

Krawczyk, C.M., Polom, U., Trabs, S., Dahm, T., 2011. Sinkholes in the city of Hamburg—new urban shear-wave reflection seismic system enables high-resolution imaging of subrosion structures. J. Appl. Geophys. 78, 133–143.

Lamont-Black, J., Baker, A., Younger, P.L., Cooper, A.H., 2005. Utilising seasonal variations in hydrogeochemistry and excitation–emission fluorescence to develop a conceptual groundwater flow model with implications for subsidence hazards: an example from Co. Durham, UK. Environ. Geol. 48, 320–335.

Marcak, H., Golebiowski, T., Tomecka-Suchon, S., 2008. Geotechnical analysis and 4D GPR measurements for the assessment of the risk of sinkholes occurring in a Polish mining area. Near Surf. Geophys. 6 (4), 233–243.

Margiotta, S., Negri, S., Parise, M., Valloni, R., 2012. Mapping the susceptibility to sinkholes in coastal areas, based on stratigraphy, geomorphology and geophysics. Nat. Hazards 62, 657–676.

Marinelli, O., 1898. Fenomeni di tipo carsico nei terrazzi alluvionali della Valle del Tagliamento. Studi orografici nelle Alpi orientali. Mem. Soc. Geol. Ital. 8 (2), 415–419.

Nisio, S., Caramanna, G., Ciotoli, G., 2007. Sinkholes hazard in Italy: first results on the inventory and analysis of some case studies. In: Parise, M., Gunn, G. (Eds.), Natural And Antropogenic Hazards In Karst Areas: Recognition, Analysis And Mitigation. Geological Society, London, Special Pubblications 279, pp. 23–45.

Nordstrom, D.K., 1977. Thermochemical redox equilibria of ZoBell'ssolution. Geochim. Cosmochim. Acta 41, 1835–1841.

Parise, M., Vennari, C., 2013. A chronological catalogue of sinkholes in Italy: the first step toward a real evaluation of the sinkhole hazard. In: Land, L., Doctor, D.H., Stephenson, B. (Eds.), Proc 13th Multidisc Conference on Sinkholes and the Engineering and Environmental Impacts of Karst, Carlsbad (New Mexico, USA), 6–10 May 2013. Natl Cave Karst Res Inst, pp. 383–392.

Pepe, P., Pentimone, N., Garziano, G., Martimucci, V., Parise, M., 2013. Lessons learned from occurrence of sinkholes related to man-made cavities in a town of southern Italy. In: Land, L., Doctor, D.H., Stephenson, B. (Eds.), Proc 13th Multidisc Conf on Sinkholes and the Engineering and Environmental Impacts of Karst, Carlsbad (New Mexico, USA), 6–10 May 2013. Natl Cave Karst Res Inst, pp. 393–401.

Pepe, P., Martimucci, V., Parise, M., 2015. Geological and geophysical techniques for the identification of subterranean cavities. In: Lollino, G., Manconi, A., Guzzetti, F., Culshaw, M., Bobrowsky, P., Luino, F. (Eds.), Engineering Geology For Society And Territory vol. 5. Springer, pp. 483–487.

Petronio, L., Poletto, F., 2010. Dual signals separation in shallow borehole hydrophone data. Proceeding of 72nd EAGE Conference & Exhibition F033. Society of Petroleum Engineers, Texas, pp. 1749–1753.
Pueyo-Anchuela, O., Pocovi, J.A., Soriano, M.A., Casas-Sainz, A.A., 2009. Characterization of karst hazards from the perspective of the doline triangle using GPR — examples from Central Ebro Basin (Spain). Eng. Geol. 108, 225–236.
SISGEO, 2005. Magnet extensometer. Available at the following website, http://www.sisgeo.com/uploads/schede/schede/d111_en.pdf (Last access, January 2015).
Soriano, M.A., Simon, J.L., 1995. Alluvional dolines in the central Ebro basin, Spain: a spatial and developmental hazard analysis. Geomorphology 11, 295–309.
Steeples, D.W., Knapp, R.W., Mc Elwee, C.D., 1986. Seismic reflection investigations of sinkholes beneath interstate highway 80 in Kansas. Geophysics 51, 295–301.
Ufficio Idrografico del Magistrato delle acque, 1966. Fiume Tagliamento. Relazione sull'influenza dell'entrata in servizio degli impianti idroelettrici dell'E.N.E.L. (già S.A.D.E.), sulla falda freatica latistante al Fiume Tagliamento, da Enemonzo a Osoppo. Technical Reportp. 30.
Van Schoor, M., 2002. Detection of sinkholes using 2D electrical resistivity imaging. J. Appl. Geophys. 50, 393–399.
Venturini, C., 2009. Note illustrative della Carta Geologica d'Italia alla scala 1:50.000, Foglio 031 Ampezzo. ISPRA.
Waltham, T., Bell, F., Culshaw, M., 2005. Sinkholes and subsidence, karst and cavernous rocks in engineering and construction. Springer-Verlag Berlin Heidelberg, New York.
Wanfang, Z., 1997. The formation of sinkholes in karst mining areas in China and some methods of prevention. Environ. Geol. 31, 50–58.